VNUHCM Journal of Science and Technology Development 2026, 29(2): 4028-4036

Open Access Full Text Article

Research Article

Monte Carlo method to correct for small-angle scattering in gamma transmission measurements with a NaI(Tl) detector

Le Hoang Minh[1,2], Ngo Truong Phu[1,2], Van Thi Thu Trang[1,2,*], Tran Thien Thanh[1,2]

ABSTRACT

Gamma transmission is a prominent technique for performing nondestructive testing and material analysis, particularly high-precision thickness measurements. However, its accuracy is often compromised by small-angle scattering, in which photons deflected at shallow angles are incorrectly counted by the detector as part of the primary transmitted beam. This is especially pronounced when using common low-resolution scintillation detectors such as NaI(Tl). This study presents a Monte Carlo simulation method, developed with the MCNP-CP software, to correct for the influence of small-angle scattering in gamma transmission measurements. The method is demonstrated using simulations of a standard experimental setup with a 2 × 2 inch NaI(Tl) detector and a collimated gamma-ray beam from three distinct radioisotope sources covering a broad energy spectrum: Co-60 (1173 and 1332 keV), Cs-137 (662 keV), and Am-241 (59.54 keV). By computationally isolating directly transmitted photons from the scattered component, the true linear attenuation coefficients are obtained for various single-element materials, including carbon, copper, and aluminum. The results demonstrate a significant improvement in accuracy; after applying the correction, the calculated attenuation coefficients deviate by less than 3% from the established NIST XCOM reference values, compared with a 6% discrepancy observed without correction. It is also found that the intensity of small-angle scattering has a complex dependence on material thickness, initially increasing to a peak before gradually declining. Analysis of the buildup factor confirms that it has a direct positive correlation with sample thickness, reflecting the increasing contribution of scattered photons in thicker materials. The behavior of the buildup factor is also strongly energy dependent: it is minimal at low energies (Am-241), shows the greatest sensitivity to the collimator's diameter at intermediate energies (Cs-137), and converges at high energies (Co-60). This work provides a validated method to enhance the precision of gamma-ray measurement systems by compensating for systematic scattering deviations.

Key words: buildup factor, linear attenuation coefficient, scattering correction, MCNP-CP, nondestructive testing

[1]*Department of Nuclear Physics, Faculty of Physics and Engineering Physics, University of Science, Ho Chi Minh City, Viet Nam*

[2]*Vietnam National University Ho Chi Minh City, Vietnam*

Correspondence

Van Thi Thu Trang, Department of Nuclear Physics, Faculty of Physics and Engineering Physics, University of Science, Ho Chi Minh City, Viet Nam

Vietnam National University Ho Chi Minh City, Vietnam

Email: vtttrang@hcmus.edu.vn

History

- Received: 05-09-2025
- Revised: 13-11-2025
- Accepted: 07-12-2025
- Published Online: 22-05-2026

DOI : https://doi.org/10.32508/vnuhcmj-std.v29i2.24584

Check for updates

INTRODUCTION

Gamma-ray transmission is a common nondestructive technique for material analysis and thickness gauging that is valued for its simple setup, versatility, and low maintenance costs. However, its accuracy can be compromised by small-angle Compton scattering, in which photons deflected at shallow angles are incorrectly counted by the detector as part of the unattenuated primary beam. This phenomenon is particularly pronounced when using low-resolution scintillation detectors like NaI(Tl), leading to systematic deviations in the calculated linear attenuation coefficients.

The contribution of scattered photons is usually quantified by the buildup factor, which is an important parameter in radiation shielding. Numerous studies have focused on calculating exposure and energy absorption buildup factors for various materials using computational tools. For instance, investigations on shielding bricks[1], common materials like water and concrete[2], and specialized glass systems[3] have demonstrated the reliability of software like MCNPX and the geometric progression method for these calculations[4–7]. These studies have confirmed that Monte Carlo methods are highly effective for simulating photon transport and shielding properties.

Precise thickness measurement is often essential for quality control: it can detect slight variations in material thickness due to defects. Various methods exist with distinct advantages. Gamma-ray techniques, including transmission and backscattering[8–10], offer simple setups, continuous operation, and low maintenance costs. They are also versatile, being unaffected by temperature or chemical composition. Gamma scattering is limited by saturation thickness, restricting its measurement range, whereas gamma transmission can measure a broader range. However, small-

Cite this article : Minh L H, Phu N T, Trang V T T, Thanh T T. **Monte Carlo method to correct for small-angle scattering in gamma transmission measurements with a NaI(Tl) detector**. *VNUHCM J. Sci. Technol. Dev.* 2026; 29(2):4028-4036.

angle Compton scattering can interfere with the accuracy of transmission measurements, especially with low-resolution detectors like NaI(Tl). This effect is stronger with thicker materials and larger detector collimators. In 2000, Shirakawa introduced a nonlinear model incorporating small-angle scattering in thickness measurements[11]. Later studies explored a simpler linear model to improve accuracy while minimizing complexity.

In this study, simulations were performed of a NaI(Tl) detector recording the transmission of gamma rays from Co-60, Cs-137, and Am-241 sources. NaI(Tl) is a commonly used type of detector and is particularly suitable for material thickness measurements, in both laboratory and field experimental setups. These three gamma sources cover a wide energy range. The high-energy gamma rays from Co-60 sources are suitable for thicker materials, and the low-energy gamma rays from Am-241 are well suited for investigations of thinner materials.

MATERIALS AND METHODS

Research subjects and methodology

Gamma-ray attenuation occurs through discrete interactions with matter, primarily the photoelectric effect, Compton scattering, and pair production. As a narrow beam passes through a material, the total intensity of the gamma beam decreases because of interactions with the material. Compton scattering is an inelastic collision between a gamma ray and an outer-shell electron. In this process, the gamma ray is deflected, transferring a portion of its energy to the electron, which is then ejected from the atom. The final energy $E_\gamma{}'$ of the scattered gamma ray depends on the scattering angle θ and can be calculated with the following formula:

$$E'_\gamma = \frac{E_\gamma}{1 + \frac{E_\gamma}{m_e c^2}(1 - \cos\theta)} \quad (1)$$

where $m_e c^2$ is the rest energy of an electron.

In gamma transmission measurements, a collimated radiation source emits a narrow beam, which is referred to as good geometry. Under these conditions, the gamma rays pass through a material and are attenuated, with the intensity reduction described by:

$$I = I_0 exp(-\mu x) \quad (2)$$

In this formula, I_0 and I denote the incident and transmitted gamma-ray intensities, respectively; μ (cm^{-1}) represents the linear attenuation coefficient, which depends on the energy of the gamma rays and the material's properties; and x(cm) is the thickness of the material.

When a broadened beam is used, known as poor geometry, this basic equation no longer applies. In such cases, an alternative expression must be used that includes a term $B(x, E_\gamma)$ to account for small-angle scattering effects:

$$\frac{I}{I_0} = B(x, E_\gamma) e^{-\mu x} \quad (3)$$

The extent of these effects varies between different types of detectors, which have distinct responses to direct and scattered gamma rays. The formal expression for small-angle scattering considers the total intensity I_{total}, which includes both transmitted and scattered components, and the transmitted intensity I_{trans}:

$$B(x, E_\gamma) = \frac{I_{total}}{I_{trans}} \quad (4)$$

Although the overall and transmitted intensities vary with sample thickness according to the Beer–Lambert law, as expressed in Equation (2) the small-angle scattering intensity follows a different behavior, which can be described by[12]

$$I_{scatter} = a\left[e^{\ cx} - e^{\ (b+c)x}\right] \quad (5)$$

where a, b, and c are constants obtained from fitting the curve.

Monte Carlo simulation software

MCNP-CP can perform calculations with nuclear sources based on evaluated nuclear structure data from ENSDF[13]. It includes coincidence and noncoincidence counting modes, which can be used to calculate and optimize the efficiency of both monoenergetic and multipurpose detectors in measurements involving real radiation sources. Three kinds of sources were used in the simulation: Co-60 (1173 and 1332 keV), Cs-137 (662 keV), and Am-241 (59.54 keV). The simulation configuration consisted of a gamma-ray source, positioned behind a collimator with a thickness of 9 cm and an inner diameter of 0.25 cm to restrict the emission angle. The diameter of the detector's collimator (d_{col}) was varied from 8 to 14 mm, with a thickness of 5.5 cm. The radioactive sources were cylindrical in shape, with a height of 0.2 cm and a radius of 0.2 cm. The emitted gamma rays went through transmission targets with varying thicknesses from 1 to 150 mm. The investigated target materials were aluminum, copper, and carbon. The NaI(Tl) detector had dimensions of 2×2 inches and was surrounded by an Al_2O_3 reflective layer with a

Table 1: Material composition of cells

Cell	Material	Density (g/cm3)	Explanation
1	NaI(Tl)	3.67	NaI crystal of the detector
2	Al2O3	2.0	Al2O3 reflector of the detector
3, 4, 5, 6	Al	2.699	Protective layer of the detector
7, 8, 11, 13, 17	Air	0.001205	Dry air
9, 10	Pb	11.35	Detector collimator
12, 15	Pb	11.35	Source collimator
14	Ceramic form	3.990	Gamma source
16	C Al Cu	1.7667 2.699 8.96	Transmission target

front thickness of 0.16 cm, along with an aluminum layer of 0.009 cm thickness.

In the input file of the MCNP-CP simulation, the "Mode P" option was used to simulate the transport of photons only. In addition, the F8 tally was applied to generate the pulse height distribution spectrum. Specifically, the command "F8:P i_{det} (i_{det} – {+(i_{det})+($i_{material}$)}) (i_{det} + {+(i_{det})+($i_{material}$)})" is declared to separate the total intensity, transmitted intensity, and scattered intensity. Here, i_{det} represents the cell index of the detector, and $i_{material}$ denotes the cell index of the material plate in the simulation. Each output file contains information on all three gamma spectra: the total, transmitted, and scattered intensity spectra. Using the transmitted component counts obtained from the simulation, an exponential relationship between the counts and thickness was then established for the transmitted component, similar to the form of Equation (2). The linear attenuation coefficient was determined by fitting the graph to the exponential function $y = A\exp(-Bx)$. Furthermore, the command "FT8 GEB a b c" was used to apply Gaussian broadening to the peaks in the simulated spectrum. Table 1 presents the composition of the simulated materials along with their densities and corresponding cell numbers in the simulation. Figure 1 shows the cross-sectional view and the model of the transmission measurement system of the simulation in MCNP-CP.

RESULTS AND DISCUSSION

Investigation of the linear attenuation coefficient

Figure 2 presents the simulated energy spectrum recorded by the NaI(Tl) detector after a collimated Co-60 gamma-ray beam has passed through a 50 mm thick aluminum sample. The MCNP-CP simulation allows for the total detected signal to be deconstructed into its constituent parts: the transmitted component (photons that pass through the sample without interaction) and the scattered component (photons that undergo Compton scattering within the sample before reaching the detector).

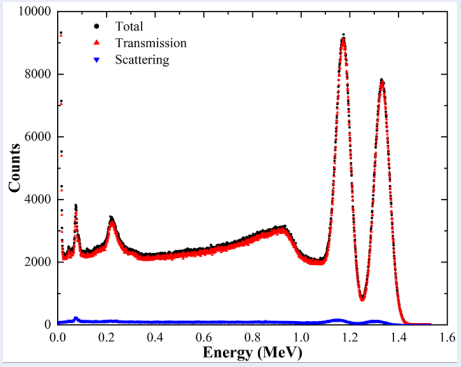

Figure 2: Simulated spectrum for a 50 mm thick aluminum sample irradiated by a Co-60 source

Figure 3 shows fitted curves for the transmitted intensity at the energy levels of 1173 and 1332 keV. The same method was applied to process the data for all remaining collimator diameters and for aluminum, carbon, and copper. For each collimator, the thickness of the samples varied from 1 to 150 mm. Table 2 shows the linear attenuation coefficients of the samples obtained before applying the correction from MCNP-CP at different energy levels, as well as the relative bias (%) between μ and the corresponding μ_{XCOM} value from the XCOM database [14].

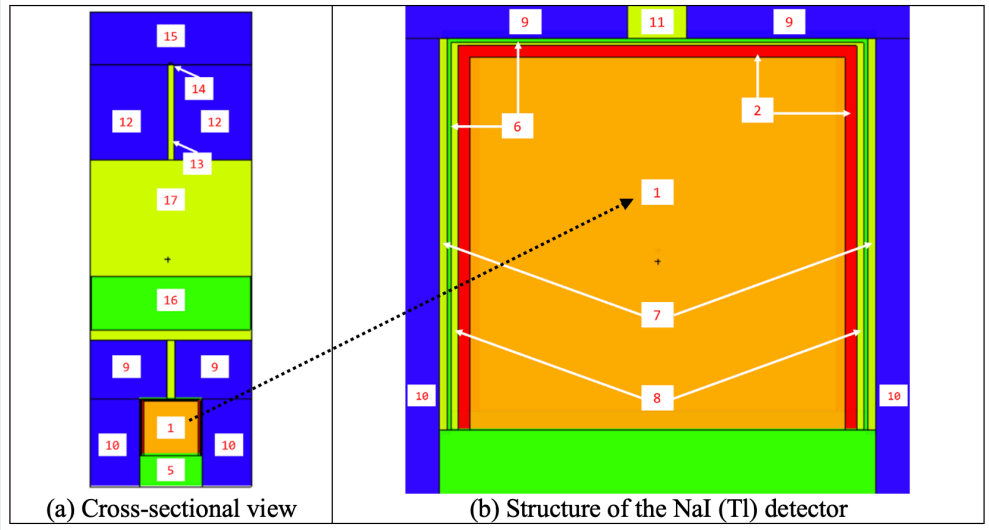

Figure 1: Schematic of the MCNP-CP simulation geometry

Table 2: Linear attenuation coefficients before correction

Sample	d_{col} (mm)	59.54 keV		662 keV		1173 keV		1332 keV	
		μ (cm^{-1})	Δ_{bias} (%)	μ (cm^{-1})	Δ_{bias} (%)	μ (cm^{-1})	Δ_{bias} (%)	μ (cm^{-1})	Δ_{bias} (%)
C	8	0.307	−1.251	0.135	−1.041	0.100	−4.038	0.095	−1.649
	10	0.306	−1.348	0.135	−1.114	0.100	−3.942	0.095	−1.649
	12	0.306	−1.477	0.135	−1.187	0.100	−3.846	0.095	−1.649
	14	0.306	−1.573	0.135	−1.261	0.100	−3.942	0.095	−1.649
Al	8	0.745	−1.765	0.199	−1.443	0.147	−4.118	0.140	−2.500
	10	0.742	−2.095	0.198	−1.542	0.147	−3.987	0.141	−2.431
	12	0.740	−2.412	0.198	−1.641	0.147	−3.987	0.140	−2.500
	14	0.738	−2.636	0.198	−1.691	0.147	−4.052	0.140	−2.500
Cu	8	14.442	−0.872	0.634	−2.569	0.459	−4.886	0.442	−2.599
	10	14.425	−0.990	0.632	−2.784	0.460	−4.845	0.442	−2.643
	12	14.397	−1.180	0.631	−2.999	0.459	−4.907	0.442	−2.731
	14	14.378	−1.313	0.630	−3.153	0.459	−5.072	0.441	−2.841

Note: Relative standard deviation $\delta\mu < 0.1\%, \triangle_{bias} = \frac{\mu - \mu_{XCOM}}{\mu_{XCOM}} \times 100\%$

Table 3: Linear attenuation coefficients after correction

Sample	d_{col} (mm)	59.54 keV		662 keV		1173 keV		1332 keV	
		μ_c (cm^{-1})	Δ_{bias} (%)	μ_c (cm^{-1})	Δ_{bias} (%)	μ_c (cm^{-1})	Δ_{bias} (%)	μ_c (cm^{-1})	Δ_{bias} (%)
C	8	0.307	−1.155	0.136	−0.234	0.102	−1.923	0.097	0.000
	10	0.307	−1.155	0.136	−0.234	0.102	−1.923	0.097	0.000
	12	0.307	−1.155	0.136	−0.234	0.102	−1.923	0.097	0.000
	14	0.307	−1.155	0.136	−0.234	0.102	−1.923	0.097	0.000
Al	8	0.745	−1.699	0.200	−0.748	0.150	−1.961	0.143	−0.694
	10	0.743	−1.963	0.200	−0.748	0.151	−1.307	0.143	−0.694
	12	0.741	−2.227	0.200	−0.748	0.151	−1.307	0.143	−0.694
	14	0.740	−2.359	0.201	−0.252	0.151	−1.307	0.143	−0.694
Cu	8	14.443	−0.865	0.641	−1.446	0.476	−1.449	0.453	−0.220
	10	14.427	−0.974	0.641	−1.446	0.476	−1.449	0.453	−0.220
	12	14.400	−1.160	0.641	−1.446	0.477	−1.242	0.453	−0.220
	14	14.381	−1.290	0.641	−1.446	0.477	−1.242	0.453	−0.220

Note: Relative standard deviation $\delta\mu < 0.1\%$,

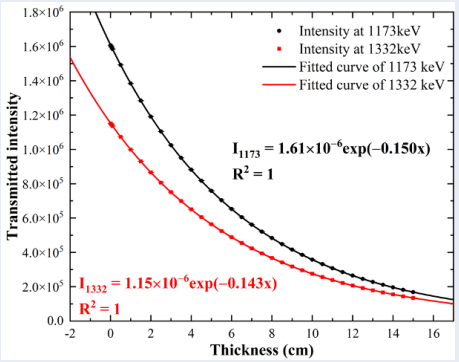

Figure 3: Simulated variation of the transmitted counts with aluminum sample thickness measured using an 8 mm collimator

Similar operations were carried out for the transmitted component to obtain the linear attenuation coefficient after performing the correction (μ_c) to separate the small-angle scattered component Table 3. Comparing the results from MCNP with the XCOM data, it can be seen that they agree closely, with the relative discrepancy not exceeding 6% for the uncorrected data and not exceeding 3% for the corrected data. Additionally, applying the fitting procedure to the MCNP simulation data yielded a highly consistent value for the linear attenuation coefficient after correction μ_c across the entire range of sample thicknesses, confirming the robustness of the method.

Correlation between variables

After verifying the accuracy of the μ_c value obtained from the MCNP-CP correction, the correlation of various quantities with the shielding material density, collimator diameter, and incident gamma-ray energy was examined. These relationships were analyzed using principal component analysis (PCA). Table 4 lists the variables considered in the PCA, namely, the material density ρ, the collimator diameter d_{col}, the incident gamma energy E, the initial intensity without shielding I_0, the corrected linear attenuation coefficient μ_c, the position of the maximum small-angle scattering component x_{max}, and the relative discrepancy between the attenuation coefficients before and after correction Bias_μ . The formulae used to determine x_{max} [12] and Bias_μ are as follows:

$$\frac{d}{d_x}(I_{scatter}) = 0 \Leftrightarrow \frac{d}{d_x}\left[a\left(e^{-cx} - e^{-(b+c)x}\right)\right] = 0 \Leftrightarrow x_{max} = \frac{1}{a_2 - a_1}\ln\frac{a_2}{a_1} \quad (6)$$

$$Bias_\mu = \left(\frac{\mu - \mu_c}{\mu_c}\right) \times 100\% \quad (7)$$

Table 4: Data for PCA evaluation

ρ (g/cm^3)	d_{col} (mm)	E (keV)	I_0	μ_c (cm^{-1})	x_{max}(cm)	Bias$_\mu$ (%)
2.6990	8	59.54	2577324	0.7452	1.4503	0
2.6990	10	59.54	3953520	0.7430	1.3725	0
2.6990	12	59.54	5444843	0.7410	1.3384	0
2.6990	14	59.54	6951317	0.7396	1.3261	0
1.7667	8	59.54	2577721	0.3073	2.9758	−1
1.7667	10	59.54	3954051	0.3072	2.8450	−1
1.7667	12	59.54	5445360	0.3069	2.7765	−1
1.7667	14	59.54	6951663	0.3068	2.7478	−1
8.9600	8	59.54	2576166	14.4431	0.0880	−2
8.9600	10	59.54	3951692	14.4268	0.0763	−2
8.9600	12	59.54	5441744	14.4001	0.0788	−2
8.9600	14	59.54	6946675	14.3813	0.0723	−2
2.6990	8	662	3496931	0.2004	3.7436	−2
2.6990	10	662	5339873	0.2004	3.5426	−2
2.6990	12	662	7361272	0.2004	3.4330	−2
2.6990	14	662	9420407	0.2005	3.3798	−2
1.7667	8	662	3494982	0.1360	4.9874	0
1.7667	10	662	5339835	0.1360	4.7048	0
1.7667	12	662	7361286	0.1361	4.5439	0
1.7667	14	662	9420363	0.1361	4.4659	0
8.9600	8	662	3495024	0.6410	1.4345	−1
8.9600	10	662	5340070	0.6410	1.3999	−1
8.9600	12	662	7361423	0.6408	1.3656	−1
8.9600	14	662	9420521	0.6408	1.3487	−1
2.6990	8	1173	1608579	0.1503	4.5879	−2
2.6990	10	1173	2286350	0.1505	4.4525	−2
2.6990	12	1173	3032747	0.1507	4.3513	−3
2.6990	14	1173	3803971	0.1507	4.2896	−3
1.7667	8	1173	1608532	0.1021	6.0528	−2
1.7667	10	1173	2286366	0.1022	5.8669	−2
1.7667	12	1173	3032810	0.1023	5.7256	−2
1.7667	14	1173	3804036	0.1023	5.6285	−2
8.9600	8	1173	1608622	0.4757	1.8362	0
8.9600	10	1173	2286511	0.4763	1.8064	0
8.9600	12	1173	3032738	0.4767	1.7734	0
8.9600	14	1173	3803966	0.4768	1.7545	0
2.6990	8	1332	1152925	0.1431	5.0847	−1
2.6990	10	1332	1639671	0.1431	4.8501	−1
2.6990	12	1332	2179249	0.1431	4.7979	−2
2.6990	14	1332	2740198	0.1431	4.7741	−2
1.7667	8	1332	1152825	0.0971	6.7532	−3
1.7667	10	1332	1639629	0.0971	6.4265	−4
1.7667	12	1332	2179236	0.0971	6.3288	−4
1.7667	14	1332	2740289	0.0972	6.2702	−4
8.9600	8	1332	1152880	0.4531	1.9705	−2
8.9600	10	1332	1639628	0.4531	1.9233	−2
8.9600	12	1332	2179306	0.4531	1.9152	−3
8.9600	14	1332	2740208	0.4532	1.9121	−3

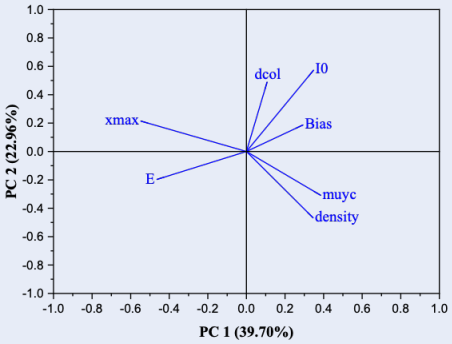

Figure 4: PCA loading plot

The PCA results in Figure 4 show that the first principal component (PC1) accounts for 39.70% of the total variance, with an eigenvalue of 2.78, making it the most significant component. The second principal component (PC2) accounts for 22.96% of the total variance, with an eigenvalue of 1.61. Therefore, together, PC1 and PC2 explain 62.66% of the total variation in the dataset. This indicates that the two-dimensional plot captures the overall data structure effectively and clearly illustrates the main relationships within the original dataset.

PC1 captures the contrast of μ_c and ρ with x_{max} and E_γ , whereas PC2 primarily represents variations driven by d_{col} and I_0 relative to μ_c and ρ. The key contributors to PC1 are μ_c, ρ, x_{max}, and E_γ , whereas for PC2, the most influential variables are d_{col}, I_0, μ_c, and ρ. The correlation analysis reveals clear patterns among the variables: μ_c and ρ exhibit a strong positive correlation, whereas I_0 shows positive associations with both Bias$_\mu$ and d_{col}. In contrast, μ_c and ρ are strongly negatively correlated with x_{max} and E_γ , with ρ and x_{max} displaying particularly strong opposition. Although E_γ and x_{max} are positively correlated, they are negatively correlated with μ_c, ρ, I_0, and Bias$_\mu$. Meanwhile, x_{max} and d_{col}, as well as E_γ and d_{col}, show little to no correlation, as indicated by their near-orthogonal positions.

The strong correlation between μ_c and ρ can be explained as follows. The linear attenuation coefficient is defined as the product of the mass attenuation coefficient and the material's density. Therefore, the loading plot accurately reflects the correlation between these two quantities. In particular, for intermediate energy levels ranging from about 100 keV to 5 MeV, Compton scattering is the dominant interaction mechanism. Since the probability of Compton scattering depends largely on the electron density, which is directly related to the material's physical density, this explains the strong relationship observed between μ_c and ρ.

The energy E_γ and the quantity x_{max} exhibit a strong positive correlation, which is consistent with the physical principle that as gamma-ray energy increases, the mean free path of gamma rays in the material also increases. That is, higher-energy gamma radiation can travel a longer distance before undergoing interaction processes. In cases where x_{max} is large, gamma rays travel a greater distance before experiencing a small-angle Compton scattering interaction.

Investigation of the buildup factor

In this subsection, the number buildup factor B is investigated. This quantity is determined by dividing the total count by the transmitted component count, as in Equation (4). for the attenuation of beam intensity. Figure 5 shows the variation of the buildup factor of the aluminum sample with thickness for several values of the collimator diameter and gamma-ray energy. It can be seen that the buildup factor increases with material thickness. When the collimator radius increases, the B factor generally tends to increase slowly. Therefore, it can be concluded that the scattered component affects the buildup factor.

At the energy level of 59.54 keV, the accumulation factor remains nearly unchanged, rising only slightly from 1.00 to about 1.012. The curves for different collimator sizes (8, 10, 12, 14 mm) are similar. At these low energies, the photoelectric effect dominates, leading to the complete absorption of photons without generating scattered photons of significant energy. As a result, few scattered photons contribute to the total spectrum, keeping the accumulation factor close to unity.

When the energy is raised to 662 keV, the accumulation factor shows a more pronounced increase with thickness, reaching about 1.023. At this energy, the separation between the curves (8–14 mm) is the greatest across all cases, indicating that the influence of the collimator slit size is strongest at this energy. Here, Compton scattering is dominant, so a significant number of photons are redirected rather than fully absorbed.

At higher energies (1173 keV and 1332 keV), the accumulation factor reaches its maximum values, peaking at about 1.045 (at 1173 keV). Despite this higher overall level, the separation between the curves (8–14 mm) is smaller than at 662 keV. Although Compton scattering continues to dominate, at these high energies, photons are primarily forward scattered at small

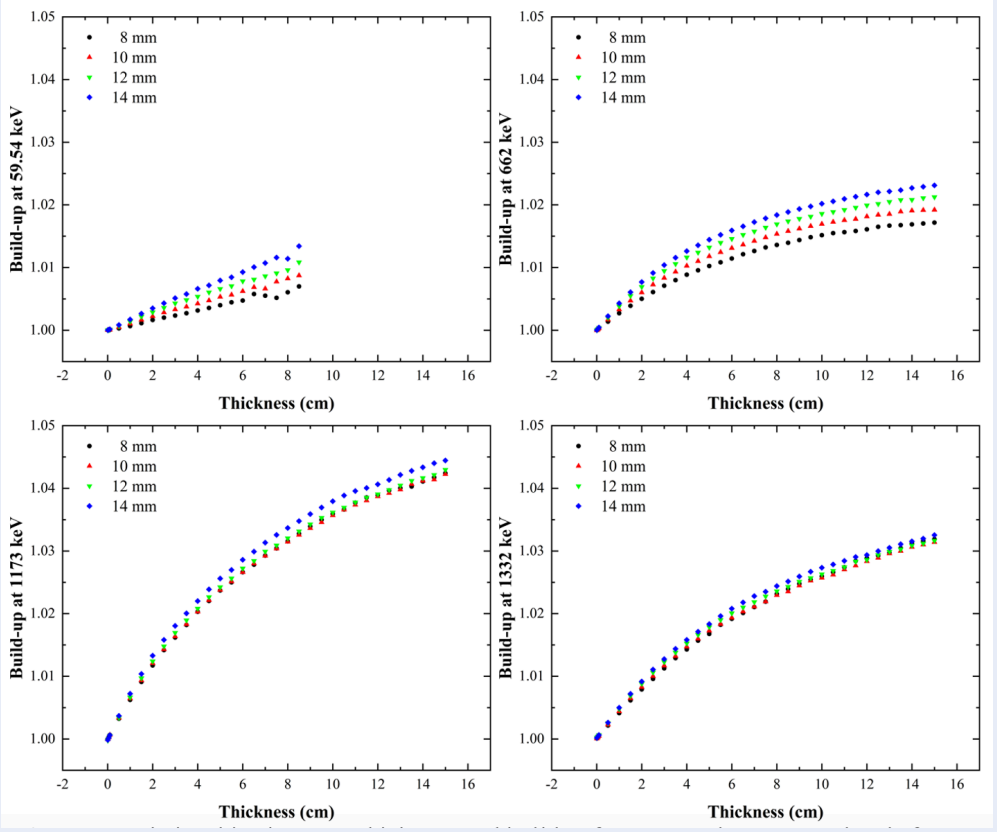

Figure 5: Relationships between thickness and buildup factor at various energy levels for an aluminum sample

angles. This reduces the effect of collimator slit size, since both narrow and wide slits can effectively capture these forward-scattered photons.

CONCLUSION

The small-angle scattering component was isolated using the extended MCNP-CP software. This allowed for the accurate determination of the linear attenuation coefficients for single-element materials, namely, carbon, aluminum, and copper. By eliminating the contribution of small-angle scattering, the accuracy of the calculated attenuation coefficients was improved, with the relative deviation from the XCOM reference data reduced to less than 3%, compared with an initial 6% discrepancy. A distinct correlation structure was observed, with two opposing variable groups: the corrected linear attenuation μ_c and the material density ρ, which are strongly correlated, and the position of maximum scattering intensity x_{max} and the incident gamma energy E_γ.

The analysis confirmed that the number buildup factor has a complex dependence on material thickness, shielding geometry, and photon energy. The correction method proved to be particularly important in the intermediate energy range (around 0.5 to 1.5 MeV), where Compton scattering is the dominant interaction mechanism and its contribution to the detected signal is largest. The size of the correction also increases in direct proportion to material thickness, as thicker samples increase the likelihood of scattering events. Conversely, at low energies (below 100 keV), where the photoelectric effect dominates, the impact of small-angle scattering is minimal.

Future work could extend this methodology to more complex scenarios, such as the analysis of multilayered or composite materials commonly found in industrial applications. This would validate the robustness of the technique for nondestructive testing of heterogeneous structures. Furthermore, a comparative experimental study using a high-resolution detector, such as a high-purity germanium detector, would be valuable. This would serve to benchmark the performance of the Monte Carlo correction by quantifying the inherently lower scattering interference in high-resolution systems.

ACKNOWLEDGEMENTS

This research is funded by Vietnam National University, Ho Chi Minh City (VNU-HCM) under grant number **B2023-18-15**.

COMPETING INTERESTS

The author(s) declare that they have no competing interests.

AUTHOR CONTRIBUTIONS

Le Hoang Minh: Conceptualization, Formal analysis, Writing - original draft. Ngo Truong Phu: Conceptualization, Formal analysis, Writing - original draft. Van Thi Thu Trang: Writing - review & editing, Funding acquisition. Tran Thien Thanh: Writing - review & editing, Project administration.

REFERENCES

1. Sayyed MI, AlZaatreh MY, Dong MG, Zaid MH, Matori KA, Tekin HO. A comprehensive study of the energy absorption and exposure buildup factors of different bricks for gamma-rays shielding. Results in Physics. 2017;7:2528–33. Available from: https://doi.org/10.1016/j.rinp.2017.07.028.
2. Olarinoye IO, Odiaga RI, Paul S. EXABCal: A program for calculating photon exposure and energy absorption buildup factors. Heliyon. 2019;5(7). Available from: https://doi.org/10.1016/j.heliyon.2019.e02017.
3. Issa SA, Tekin HO. The multiple characterization of gamma, neutron and proton shielding performances of xPbO-(99-x)B2O3–Sm2O3 glass system. Ceram Int [Internet]. Ceramics International. 2019;45(17):23561–71. Available from: https://doi.org/10.1016/j.ceramint.2019.08.065.
4. Rafiei MM, Tavakoli-Anbaran H, Kurudirek M. A detailed investigation of gamma-ray energy absorption and dose buildup factor for soft tissue and tissue equivalents using Monte Carlo simulation. Radiation Physics and Chemistry. 2020;177. Available from: https://doi.org/10.1016/j.radphyschem.2020.109118.
5. Chen R, Cammi A, Seidl M, Macian-Juan R, Wang X. Calculation of gamma-ray exposure buildup factor based on backpropagation neural network. Expert Systems with Applications. 2021;177(January). Available from: https://doi.org/10.1016/j.eswa.2021.115004.
6. Alzahrani JS, Alrowaili ZA, Olarinoye IO, Alothman MA, Al-Baradi AM, Kebaili I, et al. Nuclear shielding properties and buildup factors of Cr-based ferroalloys. Progress in Nuclear Energy. 2021;141(August). Available from: https://doi.org/10.1016/j.pnucene.2021.103956.
7. Alda'ajeh MM, Sharaf JM, Saleh HH, Hamideen MS. Determination of buildup factors for some human tissues using both MCNP5 and Phy-X / PSD. Nuclear Engineering and Technology. 2023;55(12):4426–30. Available from: https://doi.org/10.1016/j.net.2023.08.025.
8. Nguyen VH, Chuong HD, Thanh TT, Van Tao C. New method for processing gamma backscattering spectra to estimate saturation depth and to determine thickness of aluminum and steel materials. Journal of Radioanalytical and Nuclear Chemistry. 2018;315(2):293–8. Available from: https://doi.org/10.1007/s10967-017-5671-6.
9. Chuong HD, Trang LTN, Tam HD, Nguyen VH, Thanh TT. A new approach for determining the thickness of material plate using gamma backscattering method. NDT E Int [Internet]. 2020;113. Available from: https://doi.org/10.1016/j.ndteint.2020.102281.
10. Nguyen VH, Bao NH, Chuong HD, Thong ND, Thanh TT, Van Tao C. An improved semi-empirical procedure for Compton scattering technique applied to measure pipeline thickness. Journal of Radioanalytical and Nuclear Chemistry. 2021;330(3):1233–42. Available from: https://doi.org/10.1007/s10967-021-07995-3.
11. Shirakawa Y. A build-up treatment for thickness gauging of steel plates based on gamma-ray transmission. Applied Radiation and Isotopes. 2000;53(4-5):581–6. Available from: https://doi.org/10.1016/S0969-8043(00)00227-X.
12. Minh LH, Trang VT, Thanh TT. Monte Carlo approach to evaluate the small angle scattering effects in collimated beam by gamma transmission technique. Journal of Nuclear Science and Technology. 2025;62(9):1–8. Available from: https://doi.org/10.1080/00223131.2025.2480678.
13. Berlizov AN. MCNP-CP: A Correlated Particle Radiation Source Extension of a General Purpose Monte Carlo N-Particle Transport Code. CS Symposium Series. 2006;p. 183–194. Available from: https://doi.org/10.1021/bk-2007-0945.ch013;https://pubs.acs.org/doi/abs/10.1021/bk-2007-0945.ch013.
14. XCOM. XCOM: Photon Cross Sections Database [Internet]. 2010;Available from: https://physics.nist.gov/PhysRefData/Xcom/html/xcom1.html.